H. Wu et alii, Frattura ed Integrità Strutturale, 38 (2016) 99-105; DOI: 10.3221/IGF-ESIS.38.13

Focussed on Multiaxial Fatigue and Fracture

Application of the Moment Of Inertia method to the Critical-Plane Approach

Hao Wu

School of Aerospace Engineering and Applied Mechanics, Tongji University, Siping Road 1239, 200092, Shanghai, P.R.China
wuhao@tongji.edu.cn

Marco Antonio Meggiolaro, Jaime Tupiassú Pinho de Castro

Pontifical Catholic University of Rio de Janeiro, PUC-Rio, R. Marquês de São Vicente 225, Rio de Janeiro, 22451-900, Brazil
meggi@puc-rio.br, jtcastro@puc-rio.br

ABSTRACT. The Moment-Of-Inertia (MOI) method has been proposed by the authors to solve some of the shortcomings of convex-enclosure methods, when they are used to calculate path-equivalent ranges and mean components of complex non-proportional (NP) multiaxial load histories. In the proposed 2D version for use with critical-plane models, the MOI method considers the non-proportionality of the projected shear-shear history on each candidate plane through the shape of the load path, providing good results even for challenging non-convex paths. The MOI-calculated path-equivalent shear stress (or strain) ranges from each counted load event can then be used in any shear-based critical-plane multiaxial fatigue damage model, such as Findley's or Fatemi-Socie's. An efficient computer code with the shear-shear version of the MOI algorithm is also provided in this work.

KEYWORDS. Multiaxial fatigue; Non-proportional loadings; Equivalent ranges; Critical-Plane Approach.

Citation: Wu, H., Meggiolare, M.A., de Castro, J.T.P., Application of the Moment Of Inertia method to the Critical-Plane Approach, Frattura ed Integrità Strutturale, 38 (2016) 99-105.

Received: 12.05.2016
Accepted: 15.06.2016
Published: 01.10.2016

INTRODUCTION

Direction-sensitive materials like most metallic alloys tend to initiate a single dominant microcrack under fatigue loadings. Under multiaxial loading conditions this behavior tends to be well modeled by critical-plane fatigue-damage models, which search for the material plane at the critical point where the corresponding accumulated damage parameter is maximized.

Although in general any plane can be a candidate at the critical point, Bannantine and Socie [1] narrowed down the search space for the critical plane at the critical point of the structural component when it is under free-surface conditions, as usual, classifying the most common microcracks into three types, which depend on the fatigue damage mechanism: Case A tensile or Case A shear microcracks, which grow at the critical point along planes perpendicular to the free surface; and

Case B shear microcracks, which grow on planes that make an angle $\phi = 45^o$ with the free surface, see Fig. 1. To compact and hopefully clarify the critical plane notation in this work, Case A tensile planes are represented as A90(T), Case A shear as A90(S), and Case B shear as B45(S), where 90 or 45 come from their ϕ angles in degrees with respect to the free surface.

A90(T) or A90(S) microcracks only involve one normal and one shear stress/strain component, so normal or shear ranges are quite easy to calculate under variable amplitude loading (VAL) conditions using classic uniaxial rainflow procedures. However, B45(S) microcracks involve in general two shear components, an in-plane stress τ_A (or strain γ_A) and an out-of-plane τ_B (or γ_B), see Fig. 1, which must be properly combined to evaluate their joint effect on fatigue damage.

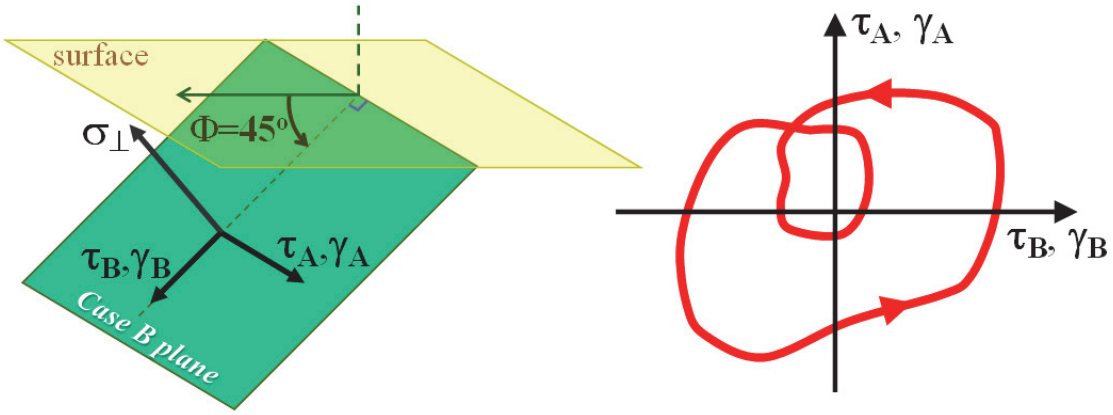

Figure 1: Non-proportional shear strain path $\gamma_B \times \gamma_A$ (or shear stress path $\tau_B \times \tau_A$) acting on a B45 candidate plane (at 45º from the free surface), for a general loading history.

The combination of both usually non-zero $\Delta\tau_B$ and $\Delta\tau_A$ ranges may cause the initiation of a combined Mode II-III B45(S) microcrack, with $\Delta\tau_B$ mainly contributing to increase its depth while $\Delta\tau_A$ is mainly tending to increase its width. The combination of $\Delta\tau_B$ and $\Delta\tau_A$ into an equivalent range $\Delta\tau$ is not a trivial step under general NP loadings, where the τ_B and the τ_A histories may be (and usually are) out of phase.

This process requires first a 2D rainflow algorithm such as the Modified Wang Brown method [2] to identify every load event from the $\tau_B \times \tau_A$ (or $\gamma_B \times \gamma_A$) history. Then, for each identified load event, its path segments are used to calculate a path-equivalent shear stress $\Delta\tau$ (or strain $\Delta\gamma$) range. The simplest approach for the $\tau_B \times \tau_A$ diagram is to assume a path-equivalent $\Delta\tau \equiv \sqrt{\Delta\tau_A^2 + \Delta\tau_B^2}$ for each identified load event, as discussed in [3].

However, this simple equivalent range expression would not be able to tell apart e.g. a rectangular from a less damaging cross-shaped $\tau_B \times \tau_A$ path with same $\Delta\tau_B$ and $\Delta\tau_A$, because both would wrongfully generate the same equivalent shear stress range $\Delta\tau$. Hence, this path-equivalent range is not a suitable solution to solve these problems in practical applications.

Another possible approach is to use the so-called convex-enclosure methods, which try to find circles, ellipses, or rectangles that circumscribe the load-event path in such 2D $\tau_B \times \tau_A$ or $\gamma_B \times \gamma_A$ diagrams. For instance, Dang Van's pioneer Minimum Ball method [4] searches for the circle with minimum radius that circumscribes each identified load path; the minimum ellipse methods [5-6] search for an ellipse with semi-axes a and b that circumscribes the entire path with minimum area $\pi \cdot a \cdot b$ or minimum "ellipse norm" $[a^2 + b^2]^{0.5}$; and the maximum rectangular hull methods search for a minimum rectangle that circumscribes the path with maximum area or maximum diagonal [7]. The value of the path-equivalent $\Delta\tau$ or $\Delta\gamma$ would be assumed as the circle diameter, the ellipse norm, or the rectangle diagonal, which is then used for fatigue damage calculation purposes.

However, such convex-enclosure algorithms do not consider the actual shape of the loading path. Instead they substitute the actual load path by some convex enclosures associated with them. Therefore, an infinite number of loading paths associated with different fatigue lives could have the same convex enclosure, wrongfully predicting the same damage if such simplified path-equivalent algorithms are used to calculate it.

This issue has been solved with the Moment-Of-Inertia (MOI) method, which has been proposed in [8-9] to estimate path-equivalent stress and strain ranges, as well as their mean components, considering the influence of the shape of the

multiaxial loading path, not only its convex enclosure. The general 6D version of the MOI is reviewed next, followed by its application in critical-plane models, proposed in this work. Further details on how the MOI works, and on its main advantages over concurrent convex-enclosure methods are studied in the aforementioned references.

THE MOMENT-OF-INERTIA (MOI) METHOD

In the MOI method, the stress or strain path is assumed to be represented by a homogeneous wire with unit mass, whose center of mass (centroid) is used to estimate the location of the mean component of the load path. Then, the mass moment of inertia (MOI) of this hypothetical wire with respect to its centroid is calculated, which gives a measure of how much the path stretches away from its mean component. The path-equivalent range of the true stress or strain path is finally calculated as a function of this MOI, which is a physically sound approximation, since paths with larger amplitudes would be associated with wider wires with increased MOI.
The MOI method has been applied to tension-torsion [10] and to general 6D histories [11], following a fatigue damage calculation approach based on stress invariants. For 6D histories, the history must first be represented in a 5D deviatoric stress or strain space, using the 5D vectors $\vec{s}'$ and $\vec{e}'$, defined as

$$\begin{cases} \vec{s}' \equiv [s_1 \quad s_2 \quad s_3 \quad s_4 \quad s_5]^T \text{ and } \vec{e}' \equiv [e_1 \quad e_2 \quad e_3 \quad e_4 \quad e_5]^T \\ s_1 \equiv \sigma_x - \dfrac{\sigma_y + \sigma_z}{2}, \quad s_2 \equiv \dfrac{\sigma_y - \sigma_z}{2}\sqrt{3}, \quad s_3 \equiv \tau_{xy}\sqrt{3}, \quad s_4 \equiv \tau_{xz}\sqrt{3}, \quad s_5 \equiv \tau_{yz}\sqrt{3} \\ e_1 \equiv \varepsilon_x - \dfrac{\varepsilon_y + \varepsilon_z}{2}, \quad e_2 \equiv \dfrac{\varepsilon_y - \varepsilon_z}{2}\sqrt{3}, \quad e_3 \equiv \dfrac{\gamma_{xy}}{2}\sqrt{3}, \quad e_4 \equiv \dfrac{\gamma_{xz}}{2}\sqrt{3}, \quad e_5 \equiv \dfrac{\gamma_{yz}}{2}\sqrt{3} \end{cases} \tag{1}$$

These deviatoric stress and strain spaces are used because they have a significant advantage over all other choices: their Euclidean norms $|\vec{s}'|$ and $|\vec{e}'|/(1+\bar{\nu})$ are equal to the von Mises equivalent stresses and strains, where $\bar{\nu}$ is an effective Poisson ratio. For 2D tension-torsion histories with stress paths defined by the normal and shear components σ_x and τ_{xy}, then $\sigma_y = \sigma_z = \tau_{xz} = \tau_{yz} = 0$, while $\varepsilon_y = \varepsilon_z = -\bar{\nu} \cdot \varepsilon_x$ and $\gamma_{xz} = \gamma_{yz} = 0$. In this case,

$$s_1 \equiv \sigma_x, \quad s_2 \equiv 0, \quad s_3 \equiv \tau_{xy}\sqrt{3}, \quad s_4 \equiv 0, \quad s_5 \equiv 0 \tag{2}$$

$$e_1 \equiv \varepsilon_x - \frac{\varepsilon_y + \varepsilon_z}{2} = \varepsilon_x \cdot (1+\bar{\nu}), \quad e_2 \equiv \frac{\varepsilon_y - \varepsilon_z}{2}\sqrt{3} = 0, \quad e_3 \equiv \frac{\gamma_{xy}}{2}\sqrt{3}, \quad e_4 = e_5 \equiv 0 \tag{3}$$

Since only s_1, s_3, e_1, and e_3 are not null, the stress or strain paths of such tension-torsion histories can be represented in the 2D deviatoric diagrams $s_1 \times s_3$ or $e_1 \times e_3$, as shown in Fig. 2.

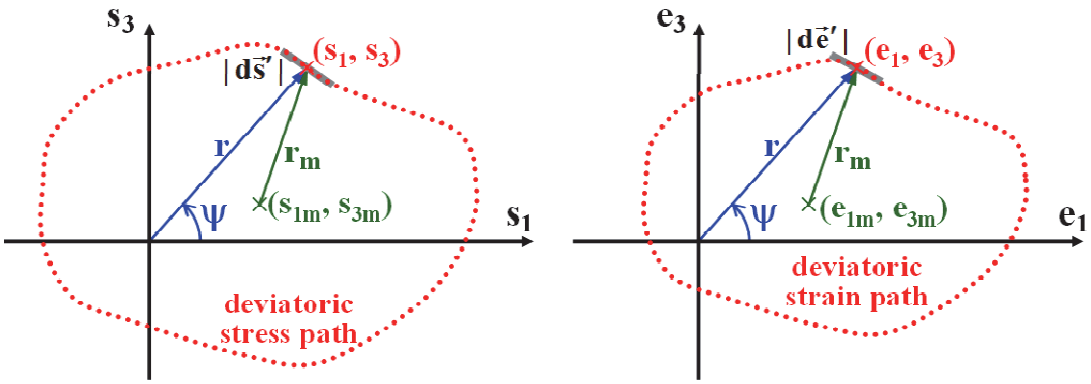

Figure 2: Stress path of a 2D tension-torsion load history in the deviatoric $s_1 \times s_3$ diagram (left) and its corresponding strain path in the $e_1 \times e_3$ diagram (right), both assumed as homogeneous wires with unit mass.

The tension-torsion version of the MOI method assumes that the 2D load path, which is represented by a series of points (s_1, s_3) or (e_1, e_3) that describe the stress or strain variations along it, is analogous to a homogeneous wire with unit mass. The mean component of the path is assumed to be located at the center of gravity of this hypothetical homogeneous wire shaped as the load history path. Its center of gravity is located at the perimeter centroid (s_{1m}, s_{3m}) or (e_{1m}, e_{3m}) of the stress or strain paths, calculated from contour integrals along it

$$s_{1m} = (1/p_s)\cdot\int s_1\cdot|d\vec{s}'|, \quad s_{3m} = (1/p_s)\cdot\int s_3\cdot|d\vec{s}'|, \quad p_s = \int|d\vec{s}'| \tag{4}$$

$$e_{1m} = (1/p_e)\cdot\int e_1\cdot|d\vec{e}'|, \quad e_{3m} = (1/p_e)\cdot\int e_3\cdot|d\vec{e}'|, \quad p_e = \int|d\vec{e}'| \tag{5}$$

where $|d\vec{s}'|$ and $|d\vec{e}'|$ are the lengths of infinitesimal segments of the stress and strain paths, while p_s and p_e are the respective path perimeters, see Fig. 2.

The MOI method calculates the path-equivalent range of a stress or strain path from the mass moment of inertia (MOI) of its corresponding unit-mass homogeneous wire. However, instead of using the axial MOI of the analogous wire, which is calculated about an *axis*, the Polar MOI (PMOI) is adopted instead, which represents the distribution of the wire (or load) path about a *single point*, its perimeter centroid. The PMOI of the stress or strain path about the perimeter centroid is then obtained from the contour integral of the square of the distance r_m between each point in the path and the path centroid, see Fig. 2, resulting in

$$I_p \equiv \frac{1}{p_s}\int\underbrace{\left[(s_1-s_{1m})^2+(s_3-s_{3m})^2\right]}_{r_m^2}|d\vec{s}'| \quad \text{or} \quad \frac{1}{p_e}\int\underbrace{\left[(e_1-e_{1m})^2+(e_3-e_{3m})^2\right]}_{r_m^2}|d\vec{e}'| \tag{6}$$

The path-equivalent ranges are assumed proportional to the radius of gyration of the path, which is equal to the square root of the PMOI of the unit-mass wire. This hypothesis is physically sound, since path segments of the load history further away from their mean components contribute more to the path-equivalent range, in the same way that wire segments further away from the perimeter centroid contribute more to the PMOI of an imaginary homogeneous wire. The path-equivalent stress and strain ranges become then

$$\Delta\sigma_{Mises} \text{ or } \Delta\varepsilon_{Mises}\cdot(1+\bar{\nu}) = \sqrt{12\cdot I_p} \tag{7}$$

THE MOI METHOD FOR THE CRITICAL-PLANE APPROACH

The MOI method has been shown experimentally to effectively estimate path-equivalent ranges [10-11]. For convex stress or strain paths, it essentially reproduces the good predictions from the Maximum Rectangular Hull method [7]. Moreover, for non-convex paths such as cross or star-shaped paths, the MOI method results in better path-equivalent ranges than any convex-enclosure method.

The 6D generalization of the MOI method can be directly used with invariant-based multiaxial fatigue damage models like Sines and Crossland. However, models based on stress or strain invariants like von Mises should not be used to make multiaxial fatigue damage predictions for directional-damage materials, like most metallic alloys, which fail due to a single dominant crack.

According to the critical-plane approach, the MOI method would lead to significant errors if directly applied to the original NP deviatoric histories, because the resulting ranges would be calculated on different planes at different points in time, not on the critical plane where the microcrack is expected to initiate under multiaxial fatigue loads. Instead of projecting the original 6D stress or strain history onto 5D deviatoric spaces, it should be projected onto the several candidate planes before proceeding with the fatigue damage analysis.

As discussed before, for directional-damage materials, the MOI method would only be needed for a B45(S) microcrack subjected to mixed Mode II-III loading, in the search for the angle θ of a candidate plane $(\theta, \phi = 45^o)$ loaded by a projected NP history combining in-plane shear stresses $\tau_A(\theta, 45^o)$ or strains $\gamma_A(\theta, 45^o)$ and out-of-plane shear stresses $\tau_B(\theta, 45^o)$ or strains $\gamma_B(\theta, 45^o)$. To do so, the load history of the two shear stresses or strains acting parallel to each B45

candidate plane first needs to be represented in a 2D $\tau_B \times \tau_A$ or $\gamma_B \times \gamma_A$ diagram, see Fig. 3, where a 2D rainflow followed by the 2D MOI method can be applied.

For each rainflow-counted path, the path perimeters p_τ or p_γ, the mean shear components (τ_{Bm}, τ_{Am}) or $(\gamma_{Bm}, \gamma_{Am})$, the associated PMOI I_p, and the resulting path-equivalent ranges $\Delta\tau$ and $\Delta\gamma$ from the MOI method become

$$p_\tau = \int \sqrt{d\tau_A^2 + d\tau_B^2}, \quad p_\gamma = \int \sqrt{d\gamma_A^2 + d\gamma_B^2} \tag{8}$$

$$\tau_{Bm} = (1/p_\tau)\cdot \int \tau_B \cdot \sqrt{d\tau_A^2 + d\tau_B^2}, \quad \tau_{Am} = (1/p_\tau)\cdot \int \tau_A \cdot \sqrt{d\tau_A^2 + d\tau_B^2} \tag{9}$$

$$\gamma_{Bm} = (1/p_\gamma)\cdot \int \gamma_B \cdot \sqrt{d\gamma_A^2 + d\gamma_B^2}, \quad \gamma_{Am} = (1/p_\gamma)\cdot \int \gamma_A \cdot \sqrt{d\gamma_A^2 + d\gamma_B^2} \tag{10}$$

$$I_p \equiv \frac{1}{p_\tau}\cdot \int \left[(\tau_B - \tau_{Bm})^2 + (\tau_A - \tau_{Am})^2\right]\cdot \sqrt{d\tau_A^2 + d\tau_B^2} \quad \text{or}$$
$$I_p \equiv \frac{1}{p_\gamma}\cdot \int \left[(\gamma_B - \gamma_{Bm})^2 + (\gamma_A - \gamma_{Am})^2\right]\cdot \sqrt{d\gamma_A^2 + d\gamma_B^2} \tag{11}$$

$$\Delta\tau \text{ or } \Delta\gamma = \sqrt{12\cdot I_p} \tag{12}$$

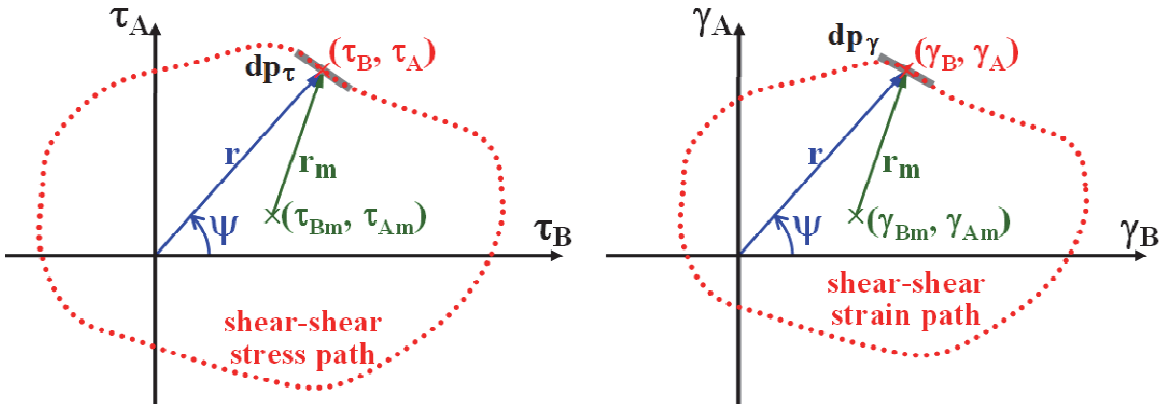

Figure 3: Stress path of a 2D shear-shear load history on a candidate plane (left) and its corresponding strain path (right), both assumed as homogeneous wires with unit mass.

For a polygonal path such as the one in Fig. 4, which is usually the case in discrete computational implementations of the MOI method, the above equations could be applied by changing the integrals into summations, and infinitesimal increments $d\tau_B$, $d\tau_A$, $d\gamma_B$, or $d\gamma_A$ into finite $\Delta\tau_{Bi}$, $\Delta\tau_{Ai}$, $\Delta\gamma_{Bi}$, or $\Delta\gamma_{Ai}$. If each polygon side i has length $\Delta\tau_{BAi} \equiv \sqrt{\Delta\tau_{Ai}^2 + \Delta\tau_{Bi}^2}$ or $\Delta\gamma_{BAi} \equiv \sqrt{\Delta\gamma_{Ai}^2 + \Delta\gamma_{Bi}^2}$, centered at (τ_{Bmi}, τ_{Ami}) or $(\gamma_{Bmi}, \gamma_{Ami})$, and associated with a mean normal $\sigma_{\perp mi}$ or $\varepsilon_{\perp mi}$, then

$$p_\tau = \sum_i \Delta\tau_{BAi}, \quad p_\gamma = \sum_i \Delta\gamma_{BAi} \tag{13}$$

$$\tau_{Bm} = (1/p_\tau)\cdot \sum_i \tau_{Bmi}\cdot \Delta\tau_{BAi}, \quad \tau_{Am} = (1/p_\tau)\cdot \sum_i \tau_{Ami}\cdot \Delta\tau_{BAi} \tag{14}$$

$$\gamma_{Bm} = (1/p_\gamma)\cdot \sum_i \gamma_{Bmi}\cdot \Delta\gamma_{BAi}, \quad \gamma_{Am} = (1/p_\gamma)\cdot \sum_i \gamma_{Ami}\cdot \Delta\gamma_{BAi} \tag{15}$$

$$\sigma_{\perp m} = (1/p_\tau)\cdot\sum_i \sigma_{\perp mi}\cdot\Delta\tau_{BAi}, \quad \varepsilon_{\perp m} = (1/p_\gamma)\cdot\sum_i \varepsilon_{\perp mi}\cdot\Delta\gamma_{BAi} \tag{16}$$

$$I_p \equiv \frac{1}{p_\tau}\cdot\sum_i\left[\Delta\tau_{BAi}^2/12 + (\tau_{Bmi}-\tau_{Bm})^2 + (\tau_{Ami}-\tau_{Am})^2\right]\cdot\Delta\tau_{BAi} \quad \text{or}$$
$$I_p \equiv \frac{1}{p_\gamma}\cdot\sum_i\left[\Delta\gamma_{BAi}^2/12 + (\gamma_{Bmi}-\gamma_{Bm})^2 + (\gamma_{Ami}-\gamma_{Am})^2\right]\cdot\Delta\gamma_{BAi} \tag{17}$$

which are calculated adding all path-segment contributions of a given cycle (or half-cycle), whose path-equivalent range is then obtained from Eq. (12). A computer implementation of the critical-plane version of the MOI method for polygonal paths is shown in the Appendix, based on the Matlab environment [12]. Further details about such procedures can be found in [13].

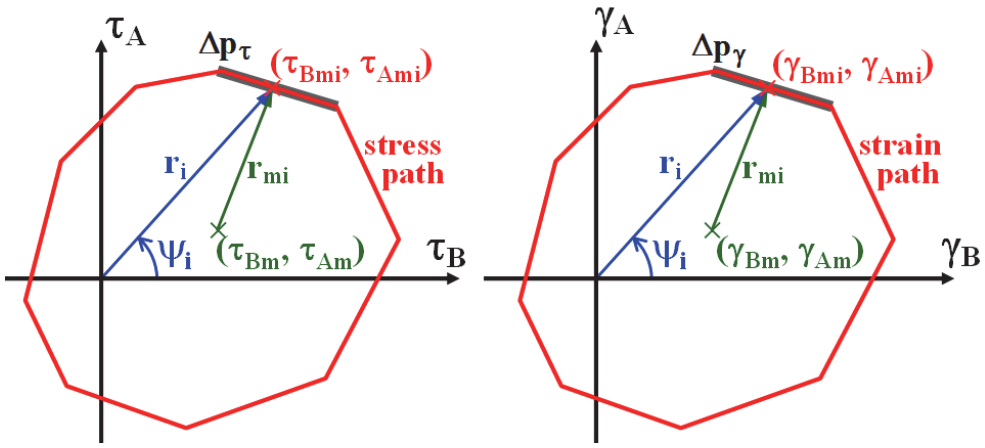

Figure 4: Polygonal shear-shear stress (left) or strain (right) paths on a candidate plane.

Conclusions

In this work, a critical-plane version of the MOI method has been presented to allow the calculation of path-equivalent shear ranges for projected shear-shear stress or strain histories on candidate planes, in multiaxial fatigue problems that must be treated by critical-plane approaches. The combination of both out-of-plane (τ_B or γ_B) and in-plane (τ_A or γ_A) shear components into an equivalent range ($\Delta\tau$ or $\Delta\gamma$) is fundamental to correctly account for shear damage on B45(S) candidate planes. The MOI method is a computationally-inexpensive and robust procedure to calculate the initiation lives of microcracks under combined in-plane and out-of-plane shear loads. The MOI method can estimate both path-equivalent ranges and mean components with a much better coherence than any convex-enclosure method. Moreover, since it accounts for the contribution of every single segment of the path, the MOI method can deal with arbitrarily shaped multiaxial load histories without losing information about such shapes.

References

[1] Bannantine, J.A., Socie, D.F., A variable amplitude multiaxial fatigue life prediction method, in: K.F. Kussmaul, D.L. McDiarmid, D.F. Socie (Eds.), Fatigue under Biaxial and Multiaxial Loading, ESIS Publication 10, London, (1991) 35-51.

[2] Meggiolaro, M.A., Castro, J.T.P., An improved multiaxial rainflow algorithm for non-proportional stress or strain histories – Part II: The Modified Wang–Brown method, Int. J. Fatigue, 42 (2012) 194-206.

[3] Castro, F.C., Araújo, J.A., Mamiya, E.N., Pinheiro, P.A., Combined resolved shear stresses as an alternative to enclosing geometrical objects as a measure of shear stress amplitude in critical plane approaches, Int. J. Fatigue, 66 (2014) 161-167.
[4] Dang Van, K., Griveau, B., Message, O., On a new multiaxial fatigue limit criterion: Theory and application, in: M. W. Brown, K. J. Miller (Eds.), Biaxial and Multiaxial Fatigue EGF3, Mechanical Engineering Publications, London, (1989) 479-496.
[5] Li, B., Santos, J.L.T., Freitas, M., A unified numerical approach for multiaxial fatigue limit evaluation, Mech. Struct. Mach., 28 (2000) 85-103.
[6] Zouain, N., Mamiya, E.N., Comes, F., Using enclosing ellipsoids in multiaxial fatigue strength criteria, European J. Mech.- A/Solids, 25 (2006) 51-71.
[7] Araújo, J.A., Dantas, A.P., Castro, F.C., Mamiya, E.N., Ferreira, J.L.A., On the characterization of the critical plane with a simple and fast alternative measure of the shear stress amplitude in multiaxial fatigue, Int. J. Fatigue, 33 (2011) 1092-1100.
[8] Meggiolaro, M.A., Castro, J.T.P., An improved multiaxial rainflow algorithm for non-proportional stress or strain histories – Part I: Enclosing surface methods, Int. J. Fatigue, 42 (2012), 217-226.
[9] Meggiolaro, M.A., Castro, J.T.P., Prediction of non-proportionality factors of multiaxial histories using the Moment Of Inertia method, Int. J. Fatigue 61, (2014) 151-159.
[10] Meggiolaro, M.A., Castro, J.T.P., The moment of inertia method to calculate equivalent ranges in non-proportional tension–torsion histories, J. Mat. Res. Tech., 4 (2015) 229-234.
[11] Meggiolaro, M.A., Castro, J.T.P., Wu, H., On the use of tensor paths to estimate the non-proportionality factor of multiaxial stress or strain histories under free-surface conditions, Acta. Mech. in press (2016).
[12] MATLAB, The MathWorks Inc., Natick, MA, (2016).
[13] Castro, J.T.P., Meggiolaro, M.A., Fatigue Design Techniques (in 3 volumes), CreateSpace, Scotts Valley, CA, USA (2016).

APPENDIX

Matlab implementation of the MOI method for a shear-shear stress history. For shear-shear strain histories, it is enough to replace all shear stress with shear strain data.

```
%INPUTS:
tauA = [0 100 100 0  0]; %single event, e.g. rectangular path in MPa
tauB = [0 0   50  50 0];

perimeter = 0; tauAm = 0; tauBm = 0; Iorigin = 0; %initialize variable
for i = 1:(size(tauA,2)-1) %for all elements of load path
  dtauA = (tauA(i+1)-tauA(i)); %increment of shear A
  dtauB = (tauB(i+1)-tauB(i)); %increment of shear B
  dtau = sqrt(dtauA^2+dtauB^2); %length of the shear increment
  perimeter = perimeter + dtau; %perimeter of the entire shear path
  tauAc = (tauA(i+1)+tauA(i))/2; %centroid of the shear A segment
  tauBc = (tauB(i+1)+tauB(i))/2; %centroid of the shear B segment
  tauAm = tauAm + dtau*tauAc; %mean of the shear A path
  tauBm = tauBm + dtau*tauBc; %mean of the shear B path
  Iorigin = Iorigin + dtau*(dtau^2/12 + tauAc^2 + tauBc^2); %PMOI
end
Iorigin = Iorigin/perimeter; %polar MOI requires division by perimeter
tauAm = tauAm/perimeter; %mean component of the shear A path
tauBm = tauBm/perimeter; %mean component of the shear B path
I = Iorigin - (tauAm^2 + tauBm^2); %PMOI with respect to path mean

%OUTPUTS:
mean_component = [tauAm tauBm] %output mean component of 2D shear path
equivalent_range = sqrt(12*I)  %output equivalent range
```